J. Fluid Mech. (1973), *vol.* 58, *part* 2, *pp.* 275–288
Printed in Great Britain

A similarity solution for slow viscous flow down an inclined plane

By PETER C. SMITH
Department of Meteorology, Massachusetts Institute of Technology

(Received 16 February 1972 and in revised form 3 October 1972)

A similarity solution is found for the distribution of layer thickness in viscous source flow down an inclined plane. With this solution at lowest order, an asymptotic expansion in inverse powers of the downstream co-ordinate x allows a small correction for upstream influence. A simple experiment confirms the major features of the similarity solution: (i) a parabolic cross-stream variation in the layer thickness; (ii) spreading of the flow according to an $x^{\frac{3}{7}}$ power law; (iii) thinning of the layer along streamlines like $x^{-\frac{1}{7}}$; and (iv) surface velocities which vary as the square of the layer thickness. Deviations of the layer-thickness measurements from the parabolic profile follow the trend predicted by the first-order corrections, whereas systematically high measured values are explained qualitatively in terms of waves at the free surface.

1. Introduction

The problem of slow viscous flow of a thin jet down an inclined plane arose in connexion with viscous-dominated bottom currents in the ocean. Classical studies of flow down inclined planes (e.g. Batchelor 1967) or of wall jets impinging on horizontal planes (e.g. Glauert 1956; Watson 1964) are generally limited to two-dimensional or axial symmetry. The analysis of the free flow of a viscous jet under gravity involves nonlinear accelerations at some point downstream of the source (Clarke 1968). However, in the present case, moderate flow rates, high viscosity and the presence of a gently sloping boundary permit the entire three-dimensional flow to remain linear. The primary balance is between the down-slope component of gravity and the retarding viscous forces. Lateral spreading of the flow is caused by the pressure gradient induced by the cross-stream variation in layer thickness. The decay of the influence of the source conditions suggests that the flow is self-similar in the downstream region.

In § 2, a single equation governing the layer thickness in the downstream region is derived from the linearized boundary-layer equations. A similarity solution is found in § 3, and two higher terms in the asymptotic expansions of the layer thickness and edge streamline are also computed. A simple experiment designed to demonstrate the validity of the similarity forms is described in § 4, and the results are discussed in § 5.

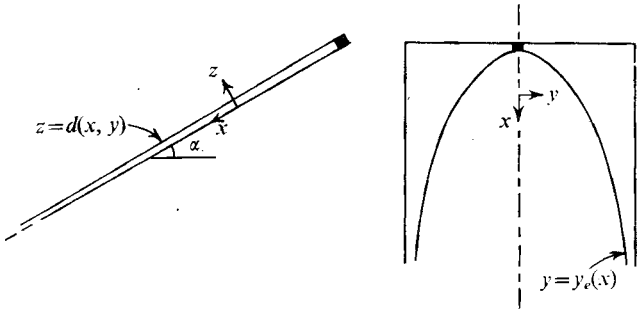

FIGURE 1. The co-ordinate system.

2. Formulation

A Cartesian co-ordinate system has been chosen with the x and y axes in the downstream and cross-stream directions respectively, and the z axis is normal to the plane. The origin is located at some arbitrary point along the axis of symmetry. The plane is inclined at an angle α to the horizontal, $z = d(x, y)$ is the upper surface of the fluid, and the edges of the flow are located at $y = \pm y_e(x)$ (see figure 1). Since only the downstream flow will be considered, the natural length scale associated with the source dimensions has been eliminated. It is standard practice in such cases to form a reference length from the external parameters of the problem: the slope $s = \tan\alpha$; viscosity ν; volumetric flow rate Q; and normal component $g' = g\cos\alpha$ of gravity. However, the asymptotic nature of the flow may be revealed by scaling the downstream co-ordinate with X_s, a measure of the distance from the source. The lack of a precise definition for X_s is justified since any length scale selected will be artificial in the sense that it cannot appear parametrically in the solution (Van Dyke 1964, p. 132). The natural scaling then follows from the definition of the downstream volumetric flow rate and the basic viscous–gravitational balance:

$$(x, y, z) = X_s(\bar{x}, \delta\bar{y}, \gamma\delta\bar{z}),$$

$$(u, v, w) = U_s(\bar{u}, \delta\bar{v}, \gamma\delta\bar{w}),$$

$$p = \rho g'\gamma\delta X_s\bar{p},$$

where
$$\delta = \left(\frac{Q\nu}{g's^4X_s^4}\right)^{\frac{1}{7}}, \quad \gamma = \left(\frac{s^3Q\nu}{g'X_s^4}\right)^{\frac{1}{7}}, \quad U_s = \left(\frac{s^5g'^3Q^4}{\nu^3X_s^2}\right)^{\frac{1}{7}}.$$

The dimensionless equations governing the steady flow of a homogeneous incompressible viscous fluid thus become

$$\bar{u}_{\bar{x}} + \bar{v}_{\bar{y}} + \bar{w}_{\bar{z}} = 0, \tag{2.1}$$

$$\bar{R}(\bar{u}\bar{u}_{\bar{x}} + \bar{v}\bar{u}_{\bar{y}} + \bar{w}\bar{u}_{\bar{z}}) = -\delta^2\bar{p}_{\bar{x}} + 1 + \bar{u}_{\bar{z}\bar{z}} + \gamma^2(\bar{u}_{\bar{y}\bar{y}} + \delta^2\bar{u}_{\bar{x}\bar{x}}), \tag{2.2}$$

$$\bar{R}(\bar{u}\bar{v}_{\bar{x}} + \bar{v}\bar{v}_{\bar{y}} + \bar{w}\bar{v}_{\bar{z}}) = -\bar{p}_{\bar{y}} + \bar{v}_{\bar{z}\bar{z}} + \gamma^2(\bar{v}_{\bar{y}\bar{y}} + \delta^2\bar{v}_{\bar{x}\bar{x}}), \tag{2.3}$$

$$\bar{R}\gamma^2(\bar{u}\bar{w}_{\bar{x}} + \bar{v}\bar{w}_{\bar{y}} + \bar{w}\bar{w}_{\bar{z}}) = -\bar{p}_{\bar{z}} - 1 + \gamma^2[\bar{w}_{\bar{z}\bar{z}} + \gamma^2(\bar{w}_{\bar{y}\bar{y}} + \delta^2\bar{w}_{\bar{x}\bar{x}})], \tag{2.4}$$

where
$$\bar{R} = (s^3Q^8/g'\nu^6X_s^{11})^{\frac{1}{7}}.$$

Next, the boundary-layer approximation is invoked by neglecting terms of quadratic order in the cross-stream aspect ratio ($\gamma^2 \ll 1$), and the flow is considered jet-like in the sense that the downstream scale far exceeds that in the cross-stream direction ($\delta^2 \ll 1$). The equations are also linearized by the assumption of a low Reynolds number ($\bar{R} \ll 1$). Note that each of these assumptions is valid for sufficiently large X_s.

Under these conditions the pressure field is hydrostatic. If the pressure components induced by surface tension at $\bar{z} = \bar{d}(\bar{x}, \bar{y})$ are ignored, the momentum equations reduce to

$$\bar{u}_{\bar{z}\bar{z}} = -1, \quad \bar{v}_{\bar{z}\bar{z}} = \bar{d}_{\bar{y}}. \tag{2.5), (2.6}$$

To the same order of approximation, the required boundary conditions are (i) the no-slip condition at the rigid surface, i.e.

$$\bar{u} = \bar{v} = \bar{w} = 0 \quad \text{at} \quad \bar{z} = 0, \tag{2.7}$$

(ii) the zero stress and kinematic conditions at the free surface

$$\left.\begin{aligned} \bar{u}_{\bar{z}} = \bar{v}_{\bar{z}} = 0 \\ \bar{w} = \bar{u}\,\bar{d}_{\bar{x}} + \bar{v}\,\bar{d}_{\bar{y}} \end{aligned}\right\} \quad \text{at} \quad \bar{z} = \bar{d}(\bar{x}, \bar{y}) \tag{2.8}$$

(2.9)

(where surface tension gradients and curvature terms of order γ^2 have been neglected) and (iii) the symmetry and edge conditions

$$\bar{d}_{\bar{y}} = 0 \quad \text{at} \quad \bar{y} = 0 \tag{2.10}$$

and

$$\bar{d} = 0 \quad \text{at} \quad \bar{y} = \pm \bar{y}_e(\bar{x}). \tag{2.11}$$

Successive integrations of (2.5) and (2.6) with respect to $\bar{z}$, using boundary conditions (2.7) and (2.8), yield parabolic velocity profiles:

$$\bar{u} = \bar{z}(\bar{d} - \tfrac{1}{2}\bar{z}) \tag{2.12}$$

and

$$\bar{v} = -\bar{d}_{\bar{y}}\bar{z}(\bar{d} - \tfrac{1}{2}\bar{z}). \tag{2.13}$$

A similar integration of the continuity equation (2.1) leads to a second-order nonlinear partial differential equation governing the distribution of layer thickness in the downstream region:

$$\bar{d}\bar{d}_{\bar{y}\bar{y}} + 3\bar{d}_{\bar{y}}^2 - 3\bar{d}_{\bar{x}} = 0. \tag{2.14}$$

Furthermore, the confinement of the flow in the lateral direction implies that the total downstream volumetric flow rate is constant:

$$\frac{Q}{\gamma\delta^2 X_s^2 U_s} = 2\int_0^{\bar{y}_e}\left(\int_0^{\bar{d}} \bar{u}\, d\bar{z}\right) d\bar{y} = \frac{2}{3}\int_0^{\bar{y}_e} \bar{d}^3\, d\bar{y} = 1. \tag{2.15}$$

3. Analysis

3.1. *Similarity solution*

An asymptotic similarity solution to (2.14) with boundary conditions (2.10) and (2.11), subject to the constraint (2.15), is sought. If the form of the similarity solution is assumed to be

$$\bar{d}(\bar{x}, \bar{y}) = f(\bar{x})\, G(\eta), \quad \text{where} \quad \eta = h(\bar{x})\, \bar{y}, \tag{3.1}$$

then (2.15) gives $f = A(a\bar{x}+b)^r$ and $h = (a\bar{x}+b)^q$ with $2q+r = -1$. The constant b results from the arbitrary location of the origin of co-ordinates, and may be eliminated by suitable redefinition. This serves to position the origin at the *effective* point source for the flow. The value of η may be normalized to one on the edge streamline, which implies that

$$\bar{y}_e(\bar{x}) = 1/h(\bar{x}) = (a\bar{x})^{-q}. \tag{3.2}$$

The downstream flux condition then provides the missing relation between the exponents:

$$\tfrac{2}{3}A^3(a\bar{x})^{-3-7q}\int_0^1 G^3\,d\eta = 1,$$

and gives $q = -\frac{3}{7}$ and $r = -\frac{1}{7}$. Free constants in the equation governing G may be eliminated by choosing $A = \frac{3}{7}a$, hence

$$GG'' + 3G'^2 + 3\eta G' + G = 0, \tag{3.3}$$

with boundary conditions

$$G'(0) = 0, \quad G(1) = 0, \tag{3.4), (3.5}$$

where a prime denotes differentiation with respect to η. The flux condition then reduces to

$$\int_0^1 G^3\,d\eta = \frac{343}{18a^3}. \tag{3.6}$$

Recognizing that (3.3) is equivalent to $[(G'+\eta)G^3]' = 0$, two integrations using (3.4) and (3.5) yield a parabolic profile for G:

$$G(\eta) = \tfrac{1}{2}(1-\eta^2). \tag{3.7}$$

Substitution into the flux condition then gives a value for a:

$$a = (5\cdot 7^4/4.3^2)^{\frac{1}{3}} = 6\cdot 9346. \tag{3.8}$$

The resulting expression for the layer-thickness distribution in dimensional form is

$$d(x,y) = \left(\frac{Q^2\nu^2}{sg'^2}\right)^{\frac{1}{7}} \frac{c}{(ax)^{\frac{1}{7}}}(1-\eta^2), \tag{3.9}$$

where $c = \frac{3}{14}a$, $\eta = y/y_e$ and

$$y_e(x) = (Q\nu/g's^4)^{\frac{1}{7}}(ax)^{\frac{3}{7}}. \tag{3.10}$$

Note that, as anticipated, the artificial length scale X_s does not appear in the result. The streamlines for the flow are lines of constant η since

$$\left(\frac{d\bar{y}}{d\bar{x}}\right)_\eta = \frac{3\bar{y}}{7\bar{x}} = -\bar{d}_{\bar{y}} = \frac{\bar{v}}{\bar{u}}. \tag{3.11}$$

Thus the solution predicts that the streamlines will spread according to an $x^{\frac{3}{7}}$ power law and that the layer thickness will diminish along streamlines like $x^{-\frac{1}{7}}$ to compensate for the spreading while maintaining constant downstream flux.

3.2. *Asymptotic theory*

In order to facilitate comparison between the similarity solution and the accompanying experiment (see § 4), it is useful to compute some higher order terms in the full asymptotic expansion of the solution. The form of the expansion in inverse powers of $\bar{x}$ is

$$\bar{d}(\bar{x},\bar{y}) = \frac{c}{(a\bar{x})^{\frac{1}{7}}}[(1-\eta^2)+\delta^2(a\bar{x})^{-\frac{8}{7}}G_1(\eta)+\bar{B}(a\bar{x})^{\lambda}H_\lambda(\eta)+\ldots], \tag{3.12}$$

where $c = \frac{3}{14}a$. Since the edge of the flow is a free streamline, its position must also be expanded in the same manner:

$$\eta_e = 1+\delta^2(a\bar{x})^{-\frac{8}{7}}\eta_{e1}+(a\bar{x})^{\lambda}\zeta_\lambda+\ldots. \tag{3.13}$$

The second term in each expansion represents a correction to the similarity solution which incorporates terms of order δ^2 in both the equations of motion and the flux condition. Under the transformation $r = \eta^2$, the equation governing G_1 takes the form of an inhomogeneous hypergeometric equation whose complementary solutions are singular at $r = 1$. Therefore, only the particular solution is physically acceptable and is found to be a fourth-order polynomial

$$G_1(\eta) = -\tfrac{1}{9}c^2(3-2\eta^2-49\eta^4). \tag{3.14}$$

The corresponding perturbation to the edge streamline comes from the boundary condition applied at $\eta^2 = 1$,

$$\eta_{e1} = \tfrac{1}{2}G_1(1) = \tfrac{8}{3}c^2. \tag{3.15}$$

The third term in each expression constitutes a departure from the asymptotic expansion in δ^2 represented by the first two terms. According to Riley (1961), there exist, in problems such as this, disturbance eigensolutions which enter the full asymptotic expansion of the solution at some order.† With the form of the perturbation defined by (3.12), $\bar{B}$ is an arbitrary amplitude of the eigenfunction H_λ and λ is a typical eigenvalue. Again using the transformation $r = \eta^2$, the general solution for H_λ is found to consist of hypergeometric functions:

$$H_\lambda(\eta) = DF(\alpha,\beta;\tfrac{1}{2};\eta^2)+E\eta F(\alpha+\tfrac{1}{2},\beta+\tfrac{1}{2};\tfrac{3}{2};\eta^2), \tag{3.16}$$

where $\alpha+\beta = \frac{5}{2}$ and $\alpha\beta = \frac{7}{2}\lambda$. For symmetric disturbances, $E = 0$, and the eigenvalues may be determined from the behaviour of H_λ near $\eta^2 = 1$, where

$$H_\lambda \sim D(1-\eta^2)^{-2}\frac{\Gamma(\frac{1}{2})\,\Gamma(2)}{\Gamma(\alpha)\,\Gamma(\beta)}.$$

The finiteness of $H_\lambda(1)$ requires that β (or α) be a negative integer ($\beta = -n$), so

$$\lambda = -\tfrac{1}{7}n(2n+5) \quad (n = 1,2,3,\ldots). \tag{3.17}$$

The lowest eigenvalue ($n = 1$, $\lambda = -1$) gives

$$H_{-1} = 1-7\eta^2, \quad \zeta_{-1} = -3\bar{B}, \tag{3.18}$$

† The author is grateful to a referee, Dr E. J. Watson, for pointing this out, and providing the initial steps in the analysis.

where D has been set equal to one without loss of generality. It is easily verified that H_{-1} satisfies the perturbation flux condition identically; that is, the disturbance involves no net contribution to the downstream volumetric flow rate. It is also worth noting that antisymmetric eigensolutions enter the expansion at higher order ($O(\bar{x}^{-\frac{12}{7}})$) and will therefore be neglected.

Substitution of the correction fields into the asymptotic expansion yields dimensional expressions for the layer thickness and edge streamline:

$$d(x,\eta) = \left(\frac{Q^2\nu^2}{sg'^2}\right)^{\frac{1}{7}} \frac{c}{(ax)^{\frac{1}{7}}}\left[(1-\eta^2)+B(ax)^{-1}(1-7\eta^2)\right.$$
$$\left.-\left(\frac{\nu Q}{s^4 g'}\right)^{\frac{2}{7}}\frac{c^2}{9}(ax)^{-\frac{8}{7}}(3-2\eta^2-49\eta^4)+\ldots\right] \quad (3.19)$$

and
$$y_e(x) = \left(\frac{\nu Q}{s^4 g'}\right)^{\frac{1}{7}}(ax)^{\frac{3}{7}}\left[1-3B(ax)^{-1}+\left(\frac{\nu Q}{s^4 g'}\right)^{\frac{2}{7}}\frac{8c^2}{3}(ax)^{-\frac{8}{7}}+\ldots\right], \quad (3.20)$$

where $c = \frac{3}{14}a$, $\eta = y/y_e$, and $B = \bar{B}X_s$ remains undetermined. Note that the first symmetric eigensolution dominates asymptotically the correction to first order in δ^2. Also, the eigenfunction correction is found to be proportional to the derivative of the basic solution with respect to x and is therefore equivalent to shifting the origin by an amount $-7B/a$ upstream.

4. Experimental results

A simple experiment was designed to verify the predictions of the similarity solution. A viscous silicone oil (Dow Corning 200 Fluid, 500 c.s.), whose properties are given in table 1 below, was emitted from a $\frac{3}{4}$ in. tube at the upper end of a Plexiglas plane inclined at $\alpha = 10{\cdot}5°$ ($s = 0{\cdot}185$). The measured flow rate $Q = 8{\cdot}8 \pm 0{\cdot}2\,\mathrm{cm}^3/\mathrm{s}$ was maintained by a constant driving head (see figure 2). The cross-stream layer-thickness profile was measured at a point 9·4 cm downstream from the tube orifice using a needlepoint micrometer. Several thickness measurements were also made at various points along the symmetry axis.

Flow patterns were recorded photographically by multiple exposure of small pieces of electrical tape advected along the free surface. A strobe light, pulsed at 100 r.p.m., exposed the black flake against a 0·1 in. grid which lay beneath the Plexiglas surface. The edge streamline was also clearly depicted on these photographs by the shadow it cast on the graph below. A typical exposure lasted 6 s and showed the flake at 10 different points in the flow.

Substituting the values of the experimental parameters into the basic similarity solution, (3.9) and (3.10), results in explicit formulae for the layer thickness and edge streamline in the downstream region:

$$d = \frac{0{\cdot}5889}{x^{\frac{1}{7}}}(1-\eta^2)\,\mathrm{cm} \quad \text{and} \quad y_e = 3{\cdot}854x^{\frac{3}{7}}\,\mathrm{cm}, \qquad (4.1), (4.2)$$

where x and y are measured in centimetres and the origin of co-ordinates is at the mouth of the tube. The streamline patterns, as measured from the photographs, are displayed in figure 3. The average deviation of all internal streamlines

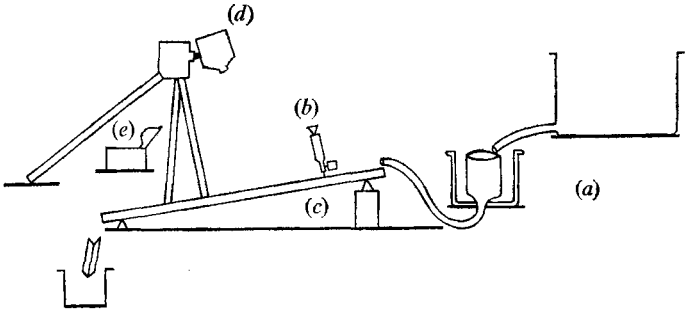

FIGURE 2. A schematic diagram of the experiment showing (*a*) constant-head device, (*b*) needlepoint micrometer, (*c*) Plexiglas plane, (*d*) camera, (*e*) strobe.

Property	Value	Source
Viscosity (ν)	$4{\cdot}86 \pm 0{\cdot}05$ cm^2/s at 72 °F	Direct measurement
Surface tension (σ)	$21{\cdot}1 \pm 0{\cdot}8$ dyne/cm at 77 °F	Published† and measured value
Density (ρ)	$0{\cdot}972 \pm 0{\cdot}001$ gm/cm^3 at 77 °F	Published† and measured value

† Dow Corning Electronics Notebook, p. 82.

TABLE 1. Properties of silicone oil (Dow 200 Fluid)

from the $x^{\frac{3}{7}}$ power law is 0·071 cm, whereas the disagreement at selected points on the edge streamline is 0·10 cm on the average. However, these discrepancies lie within the bounds of experimental error ($\pm$ 0·254 cm). The data for both the edge and several internal streamlines were normalized with respect to convenient reference values and are replotted in figure 4 to depict the spreading according to the $x^{\frac{3}{7}}$ power law more clearly.

In order to verify the expression for the surface velocity, its downstream component u_d may be integrated over the known exposure time and compared with the observed downstream displacement of the surface flake. Using the dimensional formula (3.9) for the layer thickness the expression for the downstream component of surface velocity was derived:

$$u_d = \frac{sg'}{\nu}\frac{d^2}{2} = \left(\frac{s^5 g'^3 Q^4}{\nu^3}\right)^{\frac{1}{7}} \frac{c^2}{2}(ax)^{-\frac{2}{7}}(1-\eta^2)^2. \tag{4.3}$$

Noting that $\eta = y/y_e$ is constant along the streamlines, integration yields an expression for the final downstream position x_l of the flake in terms of its initial co-ordinates (x_i, y_i) and the elapsed time Δt, i.e.

$$x_l = \frac{1}{a}\left[\left(\frac{s^5 g'^3 Q^4}{\nu^3}\right)^{\frac{1}{7}} 3c^3 \left\{1-\left(\frac{y_i}{y_{ei}}\right)^2\right\}^2 \Delta t + (ax_i)^{\frac{9}{7}}\right]^{\frac{7}{9}}. \tag{4.4}$$

The accuracy of this formula is limited mainly by observational errors in the initial co-ordinates and the small uncertainties in the flow rate Q and the viscosity ν. A comparison between predicted and measured downstream displacements is given in table 2 below. In all cases the values agree to within the bounds of experimental error.

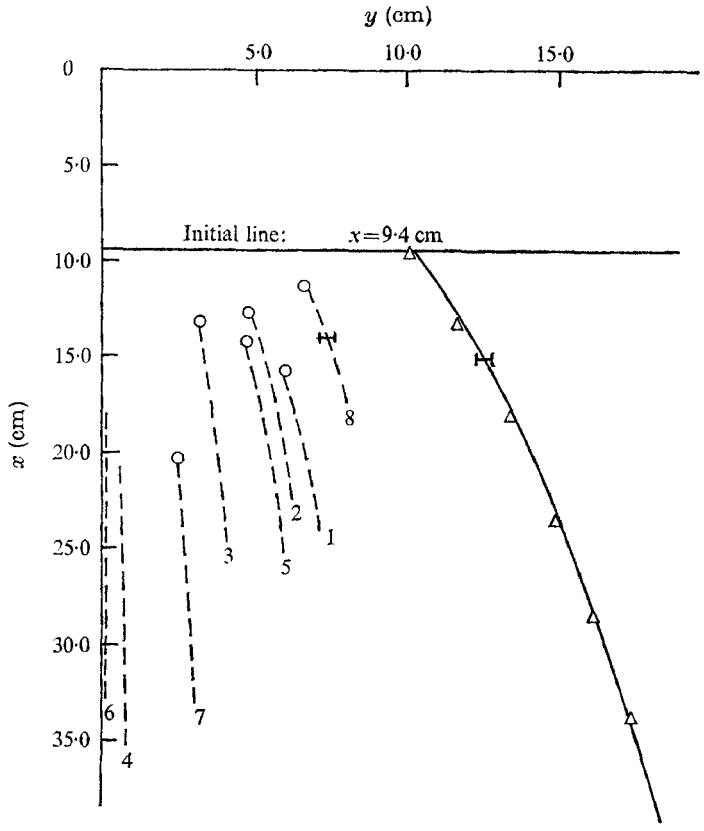

FIGURE 3. Streamline data. Solid and dashed curves are observed edge and internal streamlines. Theory: △, $y_e = 3{\cdot}854x^{\frac{3}{7}}$; ○, $y_i = (x_i/x_l)^{\frac{3}{7}}\, y_l$, where (x_i, y_i) and (x_l, y_l) are the end points of the internal streamlines.

According to the asymptotic solution (4.1) and (4.2), the characteristic dimensions of the cross-stream profile at $x_0 = 9{\cdot}4$ cm are

$$d_0 = d(x_0, 0) = 0{\cdot}428\,\text{cm} \quad \text{and} \quad y_{e0} = y_e(x_0) = 10{\cdot}07\,\text{cm},$$

as compared with measured values of 0·450 and 10·41 cm. The theoretical and measured profiles are compared in figure 5. The average deviation between the two results is 0·025 cm, which represents 5·6 % of the centre-line value. The measurements appear to be systematically higher than the predicted values, with the maximum discrepancy of 0·05 cm occurring at the edge of the flow. Despite the errors in magnitude, the layer-thickness variation is very nearly parabolic, as demonstrated by a comparison of normalized data and theory in figure 6. The downstream variation in layer thickness along the symmetry axis is shown to follow the $x^{-\frac{1}{7}}$ thinning rate in figures 7 and 8. The correspondence between the measurements and theory steadily improves with increasing downstream distance, and again the agreement between normalized data and theory is better than 3 %. However, as with the thickness profile data, systematically-high measured values are again evident. Although this trend may be removed by

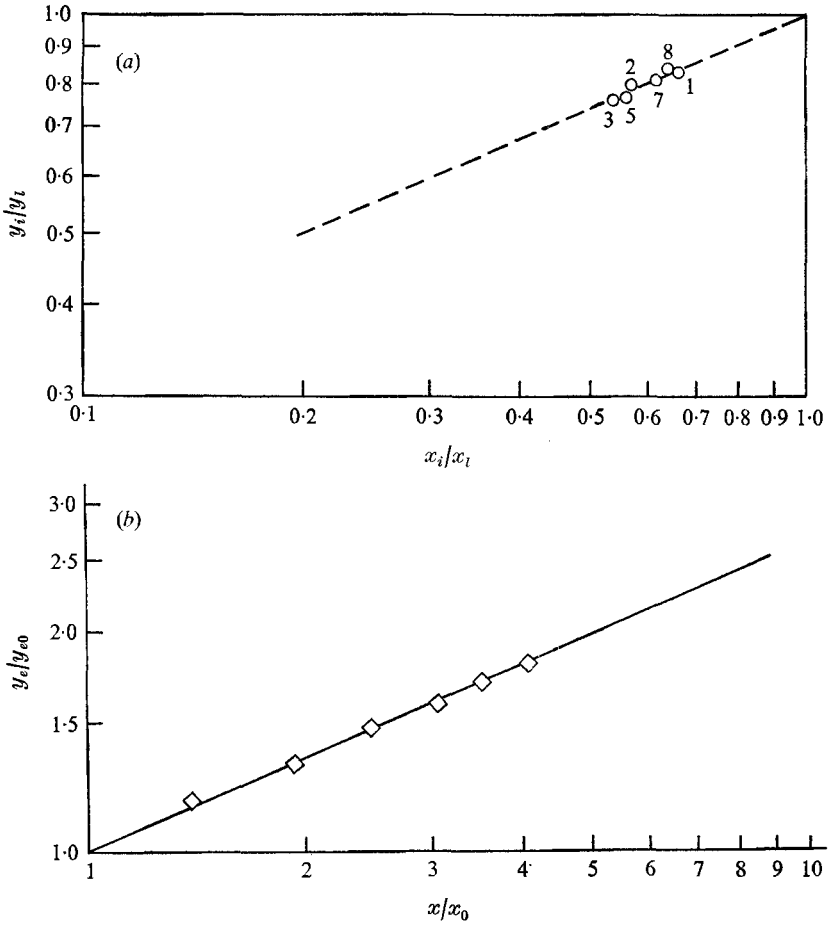

FIGURE 4. Streamline spreading by $x^{\frac{3}{7}}$ power law. (*a*) Selected internal streamlines: ○, normalized data, y_i/y_l; – – –, theory, $y_i/y_l = (x_i/x_l)^{\frac{3}{7}}$. (*b*) Edge streamline: ◇, normalized data y_e/y_{e0}, $y_{e0} = 10{\cdot}41$ cm.; ——, theory, $y_e/y_{e0} = (x/x_0)^{\frac{3}{7}}$, $y_{e0} = 10{\cdot}07$ cm, $x_0 = 9{\cdot}4$ cm.

suitable normalization, the absolute errors remain unexplained by the estimated experimental error, $\pm 0{\cdot}01$ cm.

Apart from experimental error, disagreement between the lowest order theory and measured layer-thickness profile may be attributed to the fact that the flow is not truly asymptotic at $x_0 = 9{\cdot}4$ cm. Evaluation of the scaling parameters for $X_s = x_0$ reveals that γ^2 ($= 0{\cdot}00743$) and $\bar{R}$ ($= 0{\cdot}00619$) are quite small, whereas the magnitude of δ^2 ($= 0{\cdot}217$) implies that sizeable deviations are to be expected owing to upstream influences. The non-asymptotic modifications to the thickness profile at $x = x_0$ may be calculated from (3.19):

$$\Delta d(\eta) = d_0\left[\frac{B}{ax_0}(1-7\eta^2) - \left(\frac{\nu Q}{s^4 g'}\right)^{\frac{2}{7}} \frac{c^2}{9(ax_0)^{\frac{2}{7}}}(3-2\eta^2-49\eta^4)\right], \tag{4.5}$$

where B is the unknown amplitude of the eigenfunction correction. Using observed discrepancies and (4.5) to predict an average value of B/ax_0 ($= 0{\cdot}02973$), the correction field is compared with the measured deviations from the basic

Stream-line	x_i (cm)	y_i (cm)	y_{ei} (cm)	Δt (s)	Theory x_l (cm)	Experiment x_l (cm)
1	$15{\cdot}74 \pm 0{\cdot}38$	$5{\cdot}85 \pm 0{\cdot}38$	$12{\cdot}56 \pm 0{\cdot}25$	5·4	$24{\cdot}67 \pm 1{\cdot}27$	$23{\cdot}67 \pm 0{\cdot}38$
2	$12{\cdot}70 \pm 0{\cdot}38$	$4{\cdot}82 \pm 0{\cdot}38$	$11{\cdot}45 \pm 0{\cdot}25$	5·4	$22{\cdot}93 \pm 1{\cdot}28$	$22{\cdot}10 \pm 0{\cdot}38$
3	$13{\cdot}21 \pm 0{\cdot}38$	$3{\cdot}10 \pm 0{\cdot}38$	$11{\cdot}65 \pm 0{\cdot}25$	4·8	$24{\cdot}62 \pm 0{\cdot}96$	$24{\cdot}26 \pm 0{\cdot}38$
4	$20{\cdot}83 \pm 0{\cdot}38$	$0{\cdot}51 \pm 0{\cdot}38$	$14{\cdot}16 \pm 0{\cdot}25$	6·0	$35{\cdot}52 \pm 0{\cdot}75$	$35{\cdot}10 \pm 0{\cdot}38$
5	$14{\cdot}22 \pm 0{\cdot}38$	$4{\cdot}57 \pm 0{\cdot}38$	$12{\cdot}02 \pm 0{\cdot}25$	6·0	$26{\cdot}10 \pm 1{\cdot}30$	$25{\cdot}02 \pm 0{\cdot}38$
6	$18{\cdot}03 \pm 0{\cdot}38$	$0{\cdot}05 \pm 0{\cdot}38$	$13{\cdot}31 \pm 0{\cdot}25$	5·4	$31{\cdot}77 \pm 0{\cdot}64$	$32{\cdot}63 \pm 0{\cdot}38$
7	$20{\cdot}37 \pm 0{\cdot}38$	$2{\cdot}46 \pm 0{\cdot}38$	$14{\cdot}03 \pm 0{\cdot}25$	5·4	$33{\cdot}01 \pm 0{\cdot}90$	$32{\cdot}80 \pm 0{\cdot}38$
8	$11{\cdot}30 \pm 0{\cdot}38$	$6{\cdot}65 \pm 0{\cdot}38$	$10{\cdot}90 \pm 0{\cdot}25$	5·4	$17{\cdot}62 \pm 1{\cdot}44$	$17{\cdot}40 \pm 0{\cdot}38$

TABLE 2. Integrated surface velocities

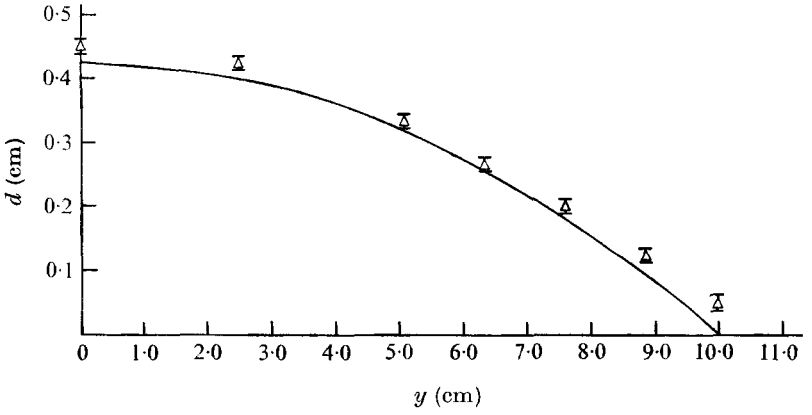

FIGURE 5. Layer-thickness profile at $x = 9{\cdot}4$ cm. △, measured values; ——, theory, $d = d_0[1-(y/y_{e0})^2]$, $d_0 = 0{\cdot}428$ cm, $y_{e0} = 10{\cdot}07$ cm.

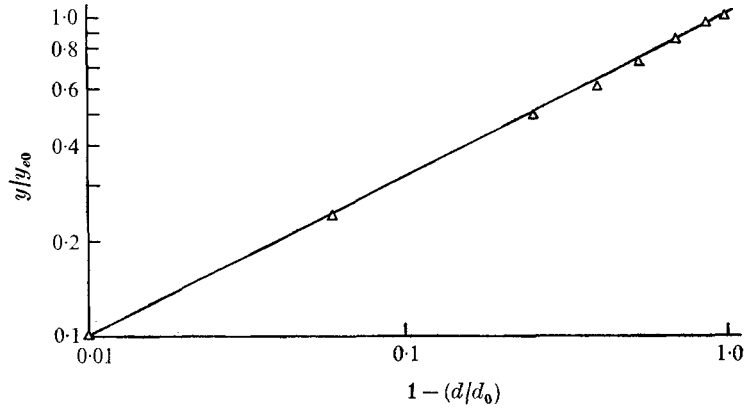

FIGURE 6. Parabolic cross-stream thickness variation. △, normalized data; ——, theory, $(1-d/d_0) = (y/y_{e0})^2$, $d_0 = 0{\cdot}428$ cm, $y_{e0} = 10{\cdot}07$ cm.

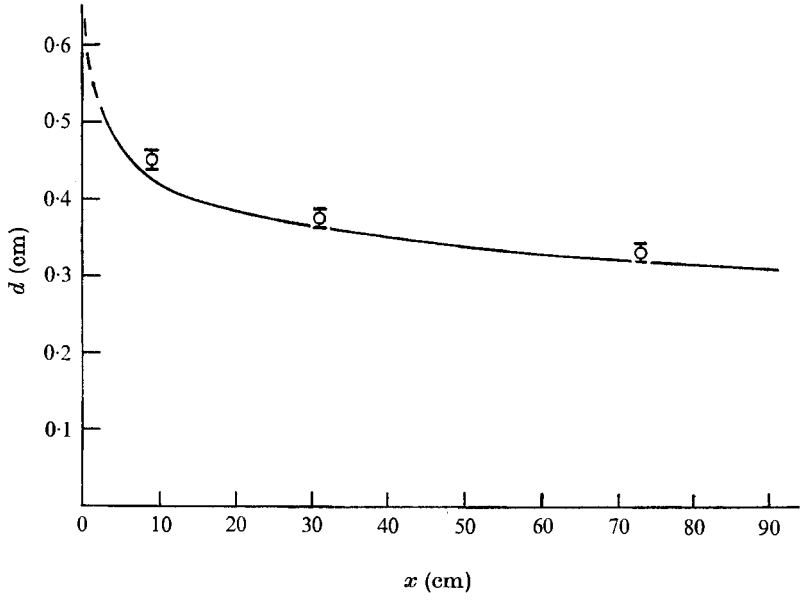

FIGURE 7. Downstream thickness variation along symmetry axis. ○, measured values; ——, theory, $d = 0{\cdot}5889x^{-\frac{1}{7}}$.

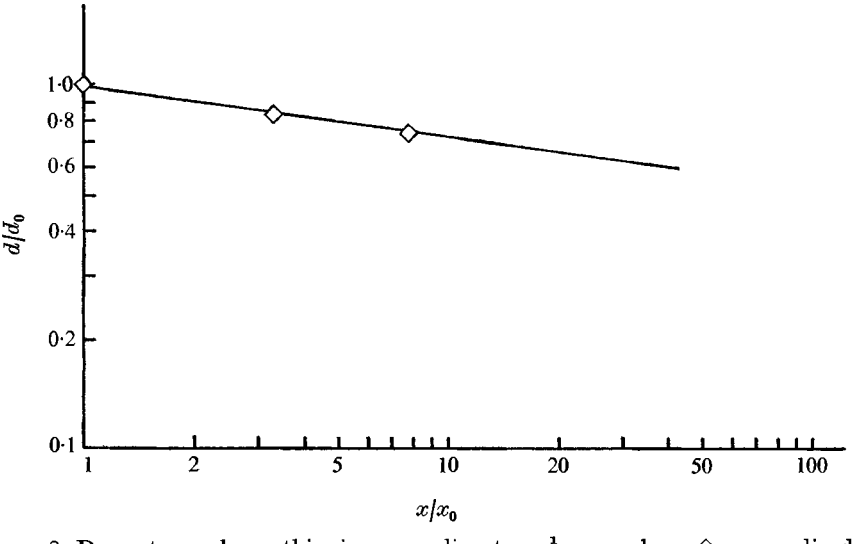

FIGURE 8. Downstream layer thinning according to $x^{-\frac{1}{7}}$ power law. ◇, normalized data; ——, theory, $d/d_0 = (x/x_0)^{-\frac{1}{7}}$, $d_0 = 0{\cdot}428$ cm, $x_0 = 9{\cdot}4$ cm.

solution in figure 9. Although the cross-stream variation of the correction profile is reproduced quite well by the theory, the measured corrections are systematically high by 0·0188 cm on the average. In addition, the perturbed position of the edge streamline is predicted to be

$$y_e = y_{e0}\left(1 - \frac{3B}{ax_0} + \left(\frac{\nu Q}{s^4 g'}\right)^{\frac{2}{7}} \frac{8c^2}{3(ax_0)^{\frac{6}{7}}}\right) = 10{\cdot}58\text{ cm}, \tag{4.6}$$

which compares favourably with the observed value of 10·41 cm.

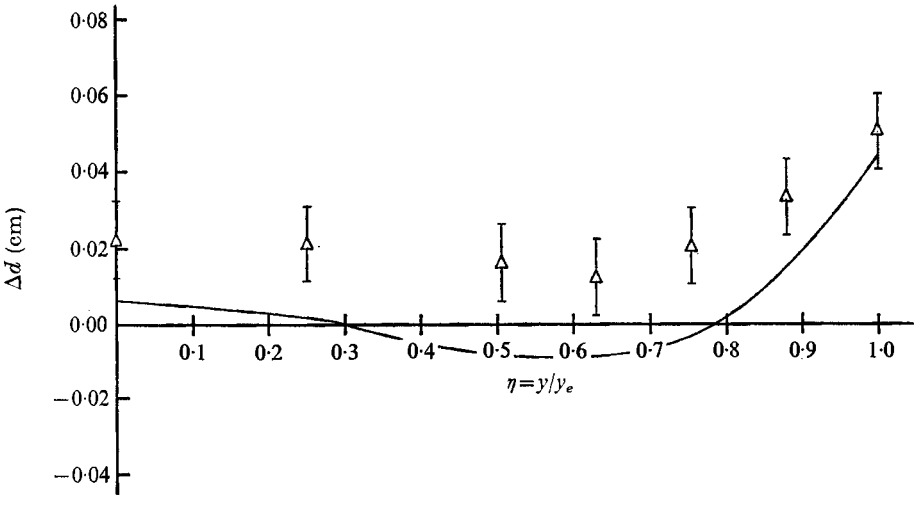

FIGURE 9. First-order corrections to layer-thickness profile at $x_0 = 9{\cdot}4$ cm. △, measured deviations from lowest order theory; ——, eigensolution plus first-order similarity correction, $\Delta d = 0{\cdot}428[(B/ax_0)(1-7\eta^2)-0{\cdot}00586(3-2\eta^2-49\eta^4)]$, $B/ax_0 = 0{\cdot}0297$.

5. Discussion

The analytical forms for the similarity solution, (3.9) and (3.10), were derived on the assumption that the origin of co-ordinates was located at the effective source for the downstream flow. In practice, the ambiguity of this ill-defined concept is compounded, since the real flow does not originate from a distinct point, but rather from an orifice of finite dimension. The apparent purpose of the eigenfunction correction is to compensate for the uncertainty introduced by positioning the origin at the physical source. The eigenfunction amplitude B derived from the layer-thickness observations at x_0 corresponds to a shift of the origin downstream by 1·96 cm. Since this determination of B is made from data contaminated by experimental error, its reliability may be questioned. However, the correction fields resulting from other trial values of B do not reflect the observed variation as well. Moreover, because of the constraint of the flux condition it would be impossible for any value of B to explain systematically-high measurements.

The theory fails to account for surface tension, but its neglect may be justified by order-of-magnitude arguments. If surface tension gradients are neglected, a scale analysis indicates that surface tension effects are felt only over very short distances

$$(\sigma/\rho g')^{\frac{1}{2}} = 0{\cdot}15\,\text{cm}. \tag{5.1}$$

Irregularities of this order were distinctly observed along the edge streamline, where the influence of surface tension is expected to be most pronounced owing to interaction with the solid plane. A rigorous treatment of surface tension in the present context leads to a singular perturbation problem in which the surface tension effects are measured by the small parameter $\epsilon = \sigma/\rho g'\delta^2 X_s^2$ ($\sim 10^{-3}$ for $X_s = x_0$), which represents the ratio of the surface tension length scale to the

cross-stream scale. However, a detailed analysis is beyond the scope of the present investigation.

Experimental error is responsible for most of the disagreement between measurement and theory. The deviations of the observed streamline trajectories from the $x^{\frac{3}{7}}$ power law may be attributed to inaccuracies in reading the positions of the surface flakes and edge streamline from the photographs. These positional errors also contribute to the uncertainty in the predicted surface velocities and downstream displacements. For the thickness measurements, the flexure of the micrometer arm when the needlepoint touched the solid plane tended to produce systematically high values. However, the estimated magnitude of this effect, 0·01 cm, cannot fully account for the observed discrepancies in figure 9. Apart from uncertainties in the parameter values, it is thought that the remaining disagreement might be related to the presence of waves at the free surface. Such waves would be produced by minor variations in the flow rate or other irregularities associated with the orific conditions. According to a stability criterion for two-dimensional flow of depth d_0 (Yih 1965, p. 180) all small waves are damped in the downstream region. This downstream damping effect is suggested by the steadily improving agreement between measurement and theory in figure 7. Nevertheless, the waves may have had sufficient amplitude at x_0 to touch the needlepoint above the mean level. However, quantitative assessment of these effects appears impossible, and they must be considered as part of the 'noise' in the measurement.

In summary, the self-similar character of source flow down an inclined plane has been demonstrated. The asymptotic layer-thickness profile is found to be parabolic, the flow spreads according to an $x^{\frac{3}{7}}$ power law and the layer thins along streamlines like $x^{-\frac{1}{7}}$. Moreover, the integrated surface velocity along streamlines accurately predicts the observed downstream displacement of surface flakes. The sum of an eigenfunction correction, whose amplitude is determined from the experimental data, and the first-order similarity correction is in close agreement with the observed deviations from the lowest order profile. Finally, a qualitative explanation in terms of waves at the free surface has been offered for the systematically high values of the measured thickness profile.

The author wishes to thank Professor H. Stommel and Professor R. C. Beardsley of M.I.T., and Dr W. McKee of Woods Hole Oceanographic Institution for their guidance and helpful criticism during the course of this study. He is also grateful to a referee, Dr E. J. Watson of the University of Manchester, England, for his enlightening comments concerning asymptotic methods. Portions of this work were supported by the National Science Foundation (Grant no. GA 30616) and the Office of Naval Research (Grant no. N00014-67-A-0204-0048).

REFERENCES

BATCHELOR, G. K. 1967 *An Introduction to Fluid Dynamics*. Cambridge University Press.

CLARKE, N. S. 1968 Two-dimensional flow under gravity in a jet of viscous liquid. *J. Fluid Mech.* **31**, 481.

GLAUERT, M. S. 1956 The wall jet. *J. Fluid Mech.* **1**, 625.

RILEY, N. 1961 Asymptotic expansions in radial jets. *J. Math. Phys.* **41**, 132.

VAN DYKE, M. 1964 *Perturbation Methods in Fluid Dynamics*. Academic.

WATSON, E. J. 1964 The radial spread of a liquid jet over a horizontal plane. *J. Fluid Mech.* **20**, 481.

YIH, C-S. 1965 *Dynamics of Nonhomogeneous Fluids*. Macmillan.